Conformational Transition Studies of Organosilane Polymers by Light and Neutron Scattering

Premal Shukla, Patricia M. Cotts,* Robert D. Miller, Thomas P. Russell, Barton A. Smith, Greg M. Wallraff, and Mark Baier

IBM Research Division, Almaden Research Center, San Jose, California 95120

P. Thiyagarajan

IPNS, Argonne National Laboratory, Argonne, Illinois 60439

Received February 27, 1991; Revised Manuscript Received May 24, 1991

ABSTRACT: The solution properties of several σ-conjugated alkyl-substituted organosilane polymers have been investigated in dilute solution using light and neutron scattering. The particle scattering functions are consistent with those calculated for a wormlike chain with a persistence length, l_{pers}, of approximately 6–7 nm. Measurements have also been done at low temperatures where thermochromic transitions are observed in the electronic absorption spectra. Interpretation of the particle scattering functions at temperatures at or below the transition regions is complicated by the presence of aggregates in the solutions. The results are similar to those observed for π-conjugated polymers such as the polydiacetylenes in solution.

Introduction

Substituted silane high polymers[1] represent a new class of radiation-sensitive materials, which are of technological interest as thermal precursors to silicon carbide, as photoinitiators in vinyl polymerizations, in photoresist applications, and as nonlinear optical materials, as the position of the absorption band may be varied by varying the substituent and/or molecular weight.[2,3] These polymers have an all-silicon backbone, with R and R′ substituents on *each* silicon, where R and R′ may be alkyl and/or aryl groups. They are thus more highly substituted than vinyl polymers, for example, and are potentially more extended. Depending on the nature of R and R′, the polymers exhibit a wide variety of properties.

The polysilanes absorb strongly in the UV (300–400 nm), both in solution and in the solid state, despite the fully saturated backbone. This phenomenon has led to the characterization of these polymers as "σ-conjugated", in contrast to π-conjugated polymers such as the polyacetylenes and polydiacetylenes. The absorption is best described as a $\sigma\sigma^*$ transition.[1] In spite of the σ-bonded nature of the backbone, there is a considerable delocalization and the electronic spectra depend on backbone conformation. Because of the relationship between conformation and electronic properties, chain conformational studies of polysilanes have been of great interest. A number of such experimental studies have been reported for the polysilanes.[5-8] Computational studies of conformational effects have been reported;[9] similar studies and effects have been observed for certain polydiacetylenes. Chain conformation studies on polydiacetylenes, which have properties related to the polysilanes, are also being carried out.[10-13]

Previously, we reported solution properties of several dialkyl-substituted polysilanes in various solvents.[14-16] The measured dimensions and molecular weights indicate that the polysilanes are substantially more extended than hydrocarbon polymers of a similar degree of polymerization. For example, the estimated Kuhn length, l_k, and characteristic ratio, C_∞, for poly(di-*n*-hexylsilane) are 6 nm and 20, respectively, in comparison to 1.8 nm and 10 for polystyrene. Although the silicon–silicon bond is long (2.35 Å), substituent interactions apparently cause significant steric hindrance to rotation. Despite the limited rotational freedom, the chains have a coillike conformation in solution at room temperature. A more detailed study of poly(di-*n*-hexylsilane) (PDNHS, or C6C6) in tetrahydrofuran, including a determination of the unperturbed dimensions from intrinsic viscosity measurements, will be reported separately.[17] Solution studies of a diaryl-substituted polysilane, poly[bis(*p*-*n*-butyl)phenylsilane] (PBPNBPS), indicated that the chain was significantly more extended than observed for the dialkyl-substituted polysilanes,[18] with estimated values for l_k and C_∞ of about 20 nm and 70, respectively.

In this study, we have investigated the effect of temperature on the equilibrium conformation of the polymer chain in dilute solution for three different dialkyl-substituted silane polymers: poly(di-*n*-hexylsilane) (C6C6), poly(*n*-propyl-*n*-hexylsilane) (C3C6), and poly(*n*-pentyl-*n*-hexylsilane) (C5C6). The structures of these three polymers are shown in Figure 1. These three dialkyl-substituted polysilanes each exhibit low-temperature transitions in their electronic absorption spectra as discussed below. As the solutions are cooled below room temperature, the absorption bands progressively narrow and shift toward *longer* wavelength. While the C6C6 polymer is observed to precipitate rapidly after the transition, the unsymmetrically substituted C3C6 and C5C6 polymers appear visually to remain in solution for up to 2 h.[19] It has been speculated in the literature that the observed transition manifested by abrupt changes in the electronic absorption spectrum for the C6C6 polymer reflects a conformational change from a coillike geometry to a rodlike one.[5] This type of single-chain conformational change has also been proposed as an explanation for the color changes observed in polydiacetylenes in solution.[12] Light and neutron scattering measurements reported for the polydiacetylenes indicate the presence of aggregates in solutions where the "rodlike" form is speculated to exist.[10,20-22] Light scattering measurements on dilute solutions of C6C6 in hexane have been carried out at low temperatures where a transition is observed in the electronic absorption spectrum.[15] Compelling evidence for aggregation in low-temperature solutions was also observed for this polymer, as will be discussed below. Changes in the depolarized scattering were also observed as the temperature was lowered. The unsymmetrically

0024-9297/91/2224-5606$02.50/0

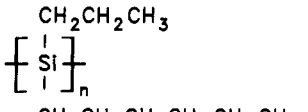

C3C6

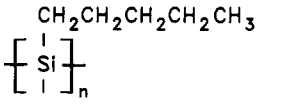

C5C6

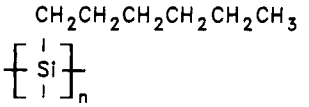

C6C6

Figure 1. Structures of the dialkylsilane polymers studied. C3C6: poly(*n*-propyl-*n*-hexylsilane). C5C6: poly(*n*-pentyl-*n*-hexylsilane). C6C6: poly(di-*n*-hexylsilane).

Table I
Summary of Intensity Light Scattering Results

polymer	solvent	dn/dc, mL/g	$10^{-6}M_w$, g/mol	10^4A_2, mL·mol/g^2	R_g, nm
C6C6	THF	0.138	2.60	1.14	92
C6C6	hexane	0.177	2.85	1.62	108
C5C6-L	THF	0.146	0.98	1.79	
C5C6-L	hexane	0.184	1.03	2.59	50
C5C6-H	THF	0.146	3.28	1.26	
C5C6-H	hexane	0.185	3.64	2.03	123
C3C6	THF	0.166	1.65	1.99	
C3C6	hexane	0.204	1.62	2.40	93

substituted C5C6 and C3C6 polymers were selected for neutron scattering measurements because of the slower precipitation observed. The neutron scattering measurements were made as the temperature was reduced through the region where the transition in the UV is observed for these polymers.

Experimental Methods

Light Scattering. Light scattering measurements in hexane and/or tetrahydrofuran (THF) were done with a Chromatix KMX-6 low-angle light scattering photometer or a Brookhaven variable-angle photogoniometer (BI200-SM). Both instruments use a 632.8-nm light source (HeNe laser). For the KMX-6, measurements were done with th 6–7° annulus and the 0.2-mm field stop. The ambient temperature results for all samples are displayed in Table I. Measurements were done under yellow lights to eliminate the photodegradation observed when the solutions are exposed to shorter wavelengths. Solutions were made by dissolving the polymers at approximately 45 °C with occasional gentle swirling of the flask. Solutions were then introduced into the light scattering cells through a syringe equipped with a stainless steel filter holder containing a 0.2-μm Fluoropore (Millipore Corp.) membrane filter to remove dust. Differential refractive index increments (dn/dc) were measured at 632.8 nm with a KMX-16 laser differential refractometer at 25 °C and are listed in Table I. The dn/dc for C6C6 differs considerably from an incorrect value reported previously.[14] Light scattering measurements below room temperature were made by circulating methanol/dry ice from a refrigerated bath through the Teflon portion of the KMX-6 cell. The KMX-6 instrument is advantageous for low-temperature measurements because of the 2-in.-thick windows in the cell, which reduce the problem of condensation significantly. Dissymmetry measurements at approximately a 180° scattering angle were made by using a reflectance accessory as reported previously.[14,23] Depolarized light scattering was measured by placing an analyzer set to the horizontal position between the cell and the detector in the KMX-6. The horizontal position of the analyzer was determined by the minimum transmission of the vertically polarized incident light.

Table II
Summary of Dynamic Light Scattering Results in Hexane

polymer	10^7D_0, cm^2/s	R_H, nm	k_D, cm^3/g	$k_D\phi$	ρ
C6C6	1.07	64.5	290	1.2	1.67
C5C6-L	2.23	31.0	228	2.9	1.61
C5C6-H	0.95	72.6	544	1.8	1.69
C4C6	1.26	54.8	393	1.6	1.70

The weight-average molecular weight, M_w, and the second virial coefficient, A_2, were evaluated from the excess scattering (the Rayleigh factor, $R_{0,c}$) at low angle (4° with the KMX-6) or zero angle (extrapolated from 15° < θ < 150° with the BI200SM), using a square-root plot to extrapolate to infinite dilution. The square-root plot has been suggested several times in the literature to minimize extrapolation errors arising from contributions of the higher order terms at the higher concentrations[24-28]

$$\left[\frac{Kc}{R_{0,c}}\right]^{1/2} = \left[\frac{1}{M_w}\right]^{1/2} + A_2M_w^{1/2}c + \dots \quad (1)$$

were $K = 4\pi^2n^2(dn/dc)^2/\lambda^4N_A$ with n the refractive index of the solution, λ the wavelength of the incident light, 623.8 nm, and N_A Avogadro's number.

Measurements of the root-mean-square radius of gyration, R_g, in hexane at ambient temperature were made by using the variable-angle goniometer over the angular range of 20° < θ < 150° to determine the initial slope of the inverse particle scattering function, $P(q)$

$$P(q) = R_{\theta,0}/R_{0,0} \quad (2)$$

$$\lim_{\theta\to 0} P^{-1}(q) = 1 + q^2R_g^2/3 + \dots \quad (3)$$

where q is the momemtum transfer vector:

$$q = (4\pi n/\lambda)\sin(\theta/2) \quad (4)$$

The initial slope may be used to determine R_g with eq 3 above independent of any assumptions about particle shape.

The hydrodynamic radius, R_H, was measured with dynamic light scattering using the BI200SM equipped with a BI 2030AT 128-channel correlator. The time correlation function, $C(t)$, was analyzed by the method of cumulants[27]

$$\ln(C(t)/B - 1)^{1/2} = \ln b^{1/2} - \bar{\Gamma}t + \mu_2t^2/2 + \dots \quad (5)$$

with B the base line of the correlation function and b an optical constant. The measured base line (average of four delay channels 1029–1032 times the sample time Δt) was used for B; however, the calculated base line obtained from the count rate was within 0.1% of the measured base line. For small q, $qR_g < 1$, the mutual diffusion coefficient at each concentration c may be obtained from the extrapolation of the reduced first cumulant, $D_c(q) \equiv \bar{\Gamma}_{c,q}/q^2$ to $q = 0$. The normalized second cumulant, $\mu_2/\bar{\Gamma}^2$, reflects the width of the molecular weight distribution. The limiting diffusion coefficient at infinite dilution, D_0, is then used to obtain R_H through the Stokes equation

$$D_0 = k_bT/6\pi\eta R_H \quad (6)$$

with k_b the Boltzmann constant, T the absolute temperature, and η the viscosity of the medium.

It should be emphasized that the samples measured here are polydisperse in molecular weight, so that the molecular parameters measured by both intensity and dynamic light scattering are averaged over this distribution. The intensity light scattering yields the weight-average molecular weight, but the root-mean-square radius of gyration and hydrodynamic radius are more complicated averages, which are not simply related to the primary moments of the molecular weight distribution. The symbols R_g

and R_H are used to indicate the experimental averages measured by light scattering

$$R_g \equiv (\langle s^2 \rangle_z)^{1/2} \tag{7}$$

where $\langle s^2 \rangle_z$ is the z-average mean-square radius of gyration, and

$$R_H \equiv \langle 1/R_H \rangle_z^{-1} \tag{8}$$

where the z-average is taken over the *inverse* hydrodynamic radius, since the experimentally measured parameter is the diffusion coefficient. These averages are not in general simply related to M_z, although in some cases, approximate relations may be obtained.

UV Absorption Spectra. The low-temperature UV measurements were done with an Oxford Instruments liquid-nitrogen cryostat. The solution concentrations were about 0.04 mg/mL. The temperature of the solution was monitored with a thermocouple immersed in the solution. Reported temperatures are estimated to be accurate to ±1.0 °C. Ultraviolet spectra were recorded on a Hewlett-Packard photodiode array spectrophotometer fitted with a neutral density and a cutoff filter to eliminate photodegradation of the polymer.

Neutron Scattering. Neutron scattering measurements were performed on the small-angle diffractometer (SAD) at the Intense Pulsed Neutron Source at the Argonne National Laboratory. Short pulses of neutrons (60–80 ns in duration) with a broad wavelength distribution (0.2–1.5 nm) are produced by positron bombardment of an enriched uranium source, with a repetition rate of 30 Hz. The neutrons scattered from the specimen are collected with a gas-filled area detector, which is used in the time-of-flight mode to generate radially averaged intensities as a function of the momemtum transfer q. Calibration of the scattering using vanadium and polystyrene standards yields the absolute differential scattering cross secretion, $d\Sigma/d\Omega$ at each q. All scattering profiles were corrected for parasitic scattering, electronic noise, and specimen attenuation in the usual manner. Experiments were performed by using a 1.5-cm-diameter aluminum sample cell with a path length of 0.1 cm. The temperature was varied and controlled by using a Displex cooling cell.

Neutron scattering, analogous to light scattering, may be used to estimate the weight-average molecular weight (M_w) and root-mean-square radius of gyration (R_g) in the Guinier region where extrapolation to $q = 0$ may be accomplished. Analogous to eqs 1 and 2, for neutrons

$$\frac{K_N c}{(d\Sigma/d\Omega)} = \frac{1}{M_w P(q)}(1 + 2A_2 c + ...) \tag{9}$$

where K_N for neutron scattering is given by

$$\frac{N_A}{m_0^2}\left(b_p - \frac{V_p}{V_s} b_s\right)^2 \tag{10}$$

with b_p and b_s the scattering lengths of the polymer repeat unit and solvent, respectively. V_p and V_s are the specific volumes of the polymer and solvent, respectively, and m_0 is the molecular weight of a repeat unit. b_p and b_s are the sums of the neutron scattering lengths for the nuclei comprising the monomer segment and solvent molecule, respectively.

Neutron scattering experiments were done for the C3C6 and C5C6 samples in deuterated hexane. The excess scattering arising from the presence of the polymer in the solvent was obtained by subtraction of the coherent scattering of the solvent and the incoherent scattering of the solvent and polymer. The incoherent scattering, assumed to be independent of scattering angle, was estimated from the scattering observed at high q.

Size Exclusion Chromatography. The molecular weight distribution was determined by size exclusion chromatography (SEC) using a Waters 150C liquid chromatograph. The mobile phase used was THF at 40 °C. The four columns contained cross-linked polystyrene beads (10-μm particle size; Polymer Laboratories) of type 10^6, 10^5, 10^4, and 10^3 Å. Approximately 0.5 mg of polymer in 250 μL of THF was injected for each sample. The concentration eluting from the column was detected by using a differential refractometer. Molecular weights relative to polystyrene at each elution volume were estimated from a calibration curve obtained from 10–15 narrow molecular weight distribution polystyrene standards. The calculations of the usual moments of the molecular weight distribution, M_w, M_n, etc., were obtained by using software from Nelson Analytical.

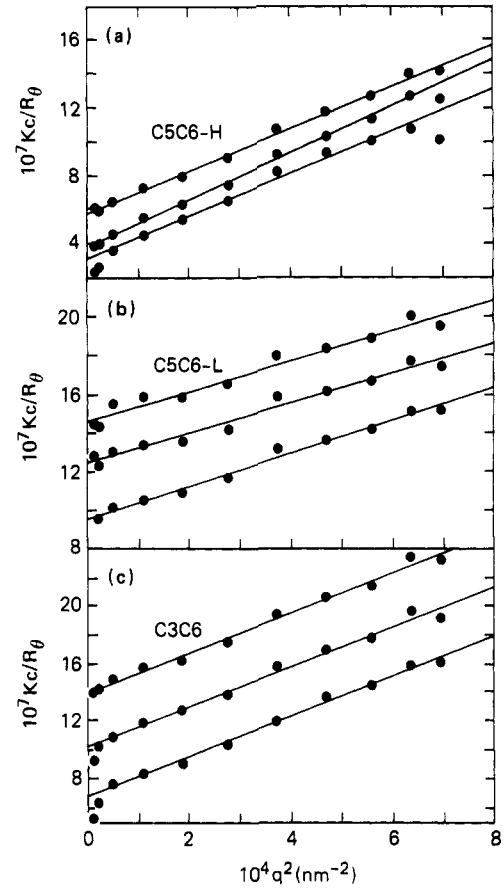

Figure 2. Kc/R_θ versus q^2 for three of the six concentrations measured for C5C6-L, C5C6-H, and C3C6 in hexane.

Results

Structure in Solution. The values of M_w, A_2, and R_g obtained by light scattering in hexane and/or THF for the samples studied are listed in Table I. The values of dn/dc are also tabulated. The angular dependence of the inverse scattering for samples C3C6, C5C6-L, and C5C6-H in hexane using the BI200SM are shown in Figure 2. Six concentrations were measured for each sample; three of the concentrations measured for each polymer are shown in Figure 2. Although the particle scattering function, $P(q)^{-1}$, for a Gaussian coil curves sharply upward for $q^2R_g^2 > 2$, the plots in Figure 2 are reasonably linear through the range of q measured, even for C5C6-H with the maximum $q^2R_g^2 = 10$. This is attributable to the breadth of the molecular weight distribution.[28] An increase in polydispersity produces a downward curvature in $P(q)^{-1}$, which balances the upward curvature.

The extrapolated zero-angle data as a function of concentration in hexane are shown in Figure 3, along with the low-angle results in THF obtained with the KMX-6. The values obtained for M_w in the two solvents using these two quite different light scattering instruments are in reasonable agreement. The values for A_2 are slightly larger in hexane than in THF. This is consistent with the slightly larger values of both R_g and the intrinsic viscosity obtained in hexane relative to THF, indicating more coil expansion due to excluded volume interactions in hexane. Data for sample C6C6 were reported previously,[14] and the values for M_w and A_2 listed in Table II for C6C6 reflect the corrected dn/dc.

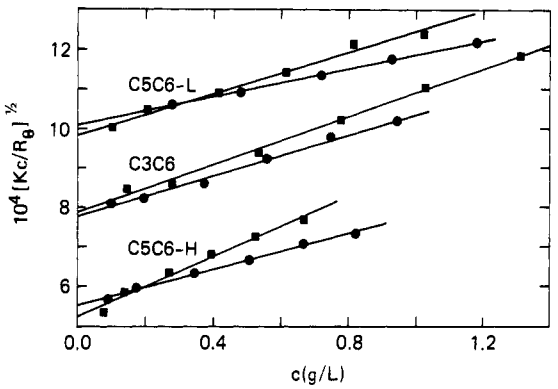

Figure 3. $[Kc/R_\theta]^{1/2}$ versus c for C5C6-H, C5C6-L, and C3C6, as indicated: (●) in THF from KMX-6, $\theta = 4°$; (■) in hexane from BI2030, extrapolated to $\theta = 0°$.

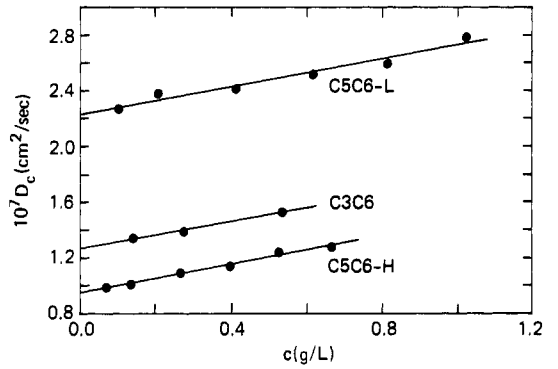

Figure 4. D_c versus c for C5C6-L, C5C6-H, and C3C6.

Table III
Summary of SEC Results

polymer	$10^{-6}M_w^{PS}$	M_w/M_n	M_z/M_w
C3C6	1.74	3.9	1.6
C5C6-L	0.92	3.2	1.6
C5C6-H	2.6	6.5	1.9
C6C6	2.2	2.3	1.7

D_c from dynamic light scattering as a function of c for C5C6-L, C5C6-H, and C3C6 in hexane is shown in Figure 4. D_c was essentially independent of q for $qR_g < 1$; consequently, only the concentration dependence is shown. A linear regression was used to obtain D_0 and k_D^c:

$$D_c = D_0(1 + k_D^c c + ...) \tag{11}$$

The values of D_0, k_D^c, and R_H are listed in Table II; those for C6C6 were reported previously. k_D^c may be put into volume fraction units using

$$k_D^\phi = Mk_D^c/N_A V_H \tag{12}$$

where

$$V_H = (4/3)\pi R_H^3 \tag{13}$$

The values of k_D^ϕ are also listed in Table III and are reasonably close to the value of approximately 2 expected for flexible, high molecular weight polymers in good solvents.

The evaluation of R_g requires no assumptions of molecular shape or conformation. Information relating to the conformation can be obtained from the dependence of R_g or R_H on M and, also, by the ratio of R_g to R_H. For the polysilanes, assuming that small changes in side-chain lengths have little or no effect on the backbone conformation in dilute solution, then the samples may be compared on the basis of their weight-average degree of polymerization, N_w, defined as $N_w = M_w/m_0$, where m_0 is the molecular weight of the repeat unit. Figure 5 shows R_g and R_H as a function of N_w for the samples studied, which can be described by the relation

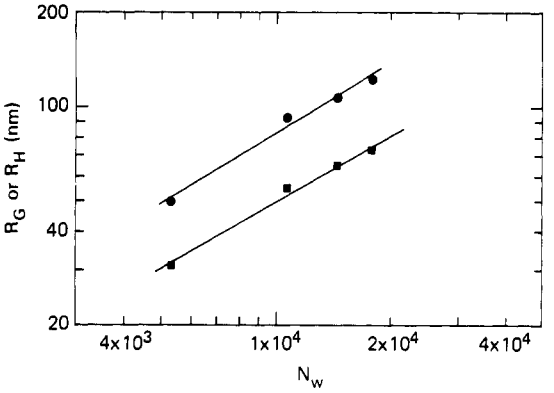

Figure 5. R_g (●) and R_H (■) versus N_w for the four dialkylpolysilanes measured, all in hexane.

$$R \propto M^\alpha \tag{14}$$

where α of approximately 0.7 was obtained for both R_g and R_H. These exponents are consistent with a random-coil polymer chain expanded in a solvent with favorable thermodynamic interactions. Alternatively, $\alpha > 0.5$ can indicate considerable stiffness of the polymer chain; however, this is not consistent with more extensive data obtained for the C6C6 polymers[14,17] or with the observation of the variation of R_g and $[\eta]$ with solvent.[29] Effects of the polymer backbone stiffness may be apparent at much lower molecular weights, or shorter length scales as discussed below. Pearson and co-workers have recently reported a stress optical coefficient that is significantly larger than those observed for carbon backbone polymers.[29]

The ratio of the radius of gyration and the hydrodynamic radius, defined as ρ

$$\rho = R_g/R_H \tag{15}$$

has been shown by Burchard and co-workers to be sensitive to polymer structure, solvent quality, and polydispersity.[30] ρ increases from the value of about 1.2–1.3 observed for narrow distribution flexible polymers in Θ-solvents with increasing chain stiffness, solvent quality, and polydispersity.[31,32] For these dialkylsilanes, $\rho = 1.67 \pm 0.04$, consistent with the good solvents hexane and THF and with the polydispersity in the molecular weight distribution.

The neutron scattering, obtained at much higher values of q, samples shorter length scales. This is advantageous for the estimation of chain stiffness because excluded-volume effects (a long-range interaction) may be neglected for $q > 0.5$ nm^{-1} and the particle scattering factor in this region is independent of M and/or sample polydispersity. In addition, the scattering functions for particles of different shape can no longer be represented by a single expression in terms of R_g such as eq 3. Thus, a model must be chosen to calculate the expected particle scattering function $P(q)$. In an ideal solvent, the Debye function for Gaussian coils is expected to be appropriate at low q, where the correlation lengths are on the order of R_g

$$P(q) = (2/u^2)(u + e^{-u} - 1) \tag{16}$$

with $u = q^2R_g^2$. At higher q where the particle scattering function becomes sensitive to the internal structure of the chain, effects of chain stiffness are apparent. At even higher q (correlation lengths of a few nanometers) the particle scattering function for a rodlike molecule will be observed. The transition from coillike to rodlike scattering

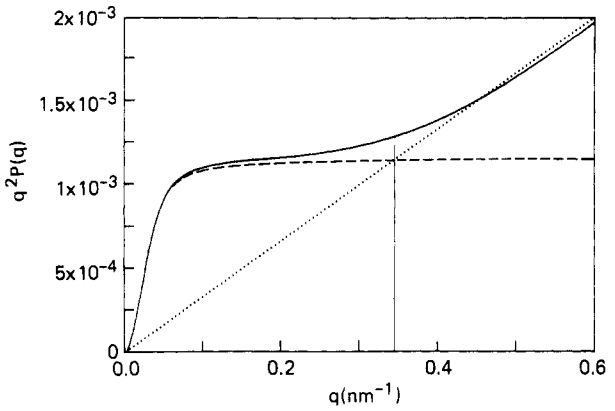

Figure 6. Kratky plots ($q^2P(q)$ versus q) for the theoretical particle scattering functions, $P(q)$, of three models: (– –) Gaussian coil (Debye function); (· · ·) rod; (—) wormlike chain.

behavior will depend on the stiffness of the chain as well as the scattering vector q. A model that encompasses both the coil and the rod in its limiting form is the Kratky–Porod wormlike chain, with the stiffness expressed in terms of the persistence length, l_{pers}.[33] In the coil limit, $l_{pers} = l_k/2$, where l_k is the Kuhn statistical segment length, and in the rod limit, $L/l_{pers} \ll 1$, where L is the contour length of the chain. An early calculation of the particle scattering function for the wormlike chain was developed by Sharp and Bloomfield;[34] however, for this study we have used the expression calculated by Koyama[35]

$$P(q) = \frac{2}{L_{red}^2} = \int_0^{L_{red}} (L_{red} - x) \exp\left\{-\frac{1}{3}(s^2 xf(x))\right\} \times \frac{\sin(sxg(x))}{sxg(x)}\,dx \quad (17)$$

where the reduced variables are

$$L_{red} = 2L/l_k; \quad s = ql_k/2; \quad x = 2t/l_k \quad (18)$$

with L the total contour length, t the contour length of a subchain, and l_k the Kuhn segment length. The functions $xf(x)$ and $xg(x)$ are defined in terms of the two moments $\langle r^2\rangle$ and $\langle r^4\rangle$ as

$$xf(x) = \frac{2\langle r^2\rangle}{l_k^2} - \frac{x^2 g(x)^2}{2} \quad (19)$$

and

$$x^2 g(x)^2 = \frac{2\langle r^2\rangle}{l_k^2}\, 10^{1/2}\left[1 - \frac{3}{5}\frac{\langle r^4\rangle}{\langle r^2\rangle^2}\right]^{1/2} \quad (20)$$

where

$$2(\langle r^2\rangle/l_k^2) = x - (1 - e^{-x}) \quad (21)$$

and

$$4(\langle r^4\rangle/l_k^4) = (5/3)x^2 - (52/9)x - (2/27)(1 - e^{-3x}) + 8(1 - e^{-x}) - 2xe^{-x} \quad (22)$$

In the limit of low q, eq 17 reduces to eq 16 above for Gaussian coils. In the limit of large q, eq 17 reduces to the particle scattering function for rods:

$$P(q) = \pi/qL \quad (23)$$

Figure 6 shows theoretical Kratky plots for the Gaussian coil, rod, and wormlike chain with $l_k = 11$ nm. At low q the wormlike chain function is identical with the coil; at high q it approaches the rodlike form. The value of $q = q^*$ at which the coil plateau and the rod asymptote intersect

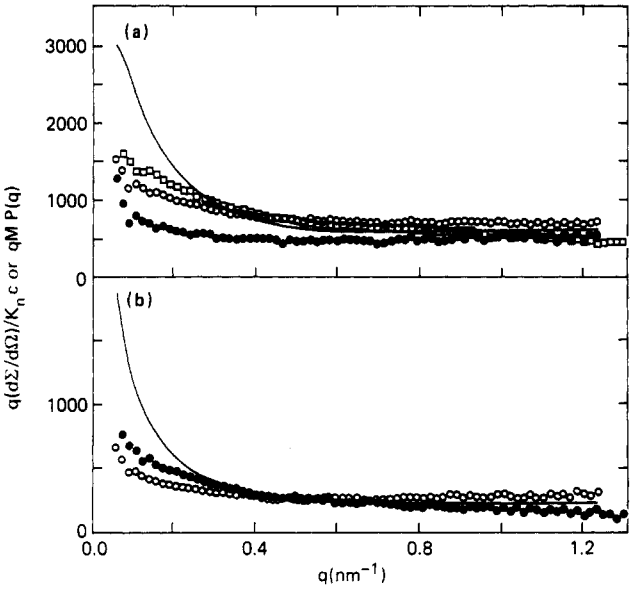

Figure 7. Holtzer plots of the experimental $q(d\Sigma/d\Omega)/K_{NC}$ (points) along with the theoretical $qMP(q)$ from the Koyama expressions for the wormlike chain with $l_k = 8$ nm (solid line). (a) (●) C5C6-H, 0.5%; (○) C5C6-L, 1%; (□) C5C6-H, 1%; (b) (●) C3C6, 1%, 1st run; (○) C3C6, 1%, 2nd run.

can in principle yield l_k:

$$q^* = 12/\pi l_k \quad (24)$$

While this point is easily distinguishable from the theoretical $P(q)$ in Figure 6, in practice the experimental data are not as easily interpreted. A more exact treatment of the scattering function for the Kratky–Porod wormlike chain given by Yoshizaki and Yamakawa[36] does not indicate the existence of a plateau region at all. The rod asymptote shown in Figure 6 has a slope equal to πM_L, where the mass per unit length $M_L \equiv M/L$, with L the length of the fully stretched out chain. In this asymptotic region, contributions from polydispersity and intermolecular interactions are insignificant. A Holtzer plot[37] of $qMP(q)$ versus q has been suggested rather than the Kratky plot to estimate M_L and l_k.[38] In this plot, the rod asymptote is horizontal, with a height equal to πM_L. Figure 7 shows plots of $q(d\Sigma/d\Omega)/K_{NC}$ versus q for C5C6-L, C5C6-H, and C3C6 as indicated. While the data scatter considerably, the rodlike plateaus at high q yield $M_L = 1900$ nm^{-1} for C5C6 and 800 nm^{-1} for C3C6. The value for C3C6 is quite similar to the M_L calculated from the unit cell dimensions from X-ray crystallography[39] (804 nm^{-1}); the value for C5C6 is anomalously high. We attribute this to the difficulty in obtaining absolute scattering intensities in neutron scattering. Figure 7 also shows the curves of $qMP(q)$ as a function of q where $P(q)$ is calculated from the Koyama theory above with M_w from light scattering and M_L from the plateau region. Both polymers are adequately described by a wormlike chain with $l_k = 8 \pm 2$ nm, for $q > 0.3$ nm^{-1}, where intermolecular interactions may be neglected. This l_k is similar to an earlier rough estimate for C6C6 of $l_k = 6 \pm 1$ nm obtained from light scattering in a good solvent with substantial approximations for effects of polydispersity and excluded-volume interactions.[14] A more precise estimation for C6C6 will be reported separately.[17] Extrapolation of the lower q data to infinite dilution could not be carried out because the samples are of very high M and the scattering contrast was too weak to be measured at lower concentrations. Thus these data are obtained at concentrations approaching the semidilute region, and data in the Guinier range cannot

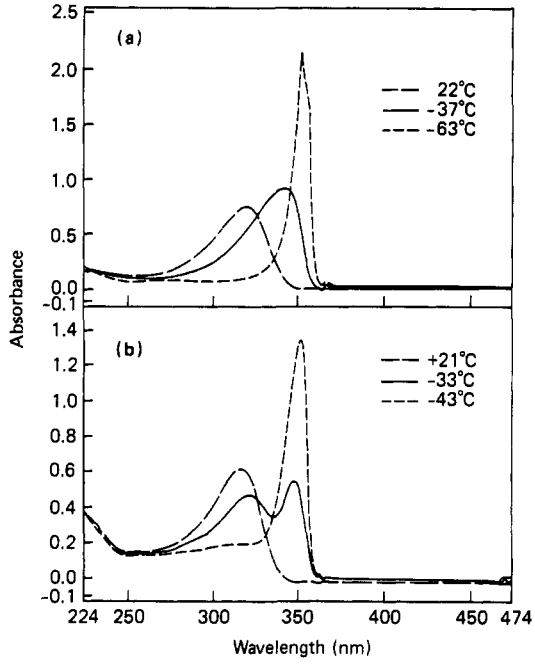

Figure 8. Electronic absorption spectra for C3C6 (a) and C5C6 (b) at the temperatures indicated.

be interpreted in terms of a single particle scattering function.

Low-Temperature Region. As mentioned above, most polysilanes exhibit thermochromism at low temperatures in the bulk and in dilute solution. Figure 8 shows examples of the changes observed as the temperature is lowered for C3C6 and C5C6 in heptane. At the lowest temperatures, where the electronic absorption band sharpens, precipitation is observed. Light scattering measurements on the C6C6 polymer were carried out at low temperatures for as low a concentration as 0.0174 g/L, or 10^{-4} M repeat units, as shown in Figure 9. This is very similar to the concentrations used in the UV absorption spectra. At this high dilution, the solution could be cooled to -32 °C before the large increase in intensity was observed. Although the estimation of R_g and M_w from a single very dilute concentration is more uncertain than the equilibrium results in Table I, we show this data to suggest a mechanism for the observed thermochromism. As the temperature is lowered from +20 down to about -10 °C, the R_g increases somewhat, consistent with the expected loss of rotational freedom. More complete measurements in this region including higher concentrations are discussed below. In the region -15 °C > T > -32 °C, R_g *decreases*, as may be seen in Figure 9. Below -32 °C, the molecular weight begins to increase rapidly as aggregates form. However, the scattering at 176° increases much less, indicating a *smaller* R_g. At higher concentrations aggregation is observed at these temperatures. These observations of a decrease in R_g at very high dilution prior to formation of multimolecular aggregates are both consistent with the *intersegmental* association, leading to shrinkage in a single chain and to aggregation among chains. At higher concentrations, only the aggregation is observed.

The large increase in scattering intensity observed at temperatures near the UV transition is indicative of phase separation in these solutions. Phase separation in polymer solutions occurs by two mechanisms: (1) a liquid–liquid separation of a more concentrated but still amorphous phase at an upper critical solution temperature (UCST) and (2) a liquid–crystal separation of a crystallizable polymer. The liquid–liquid phase separation occurs for

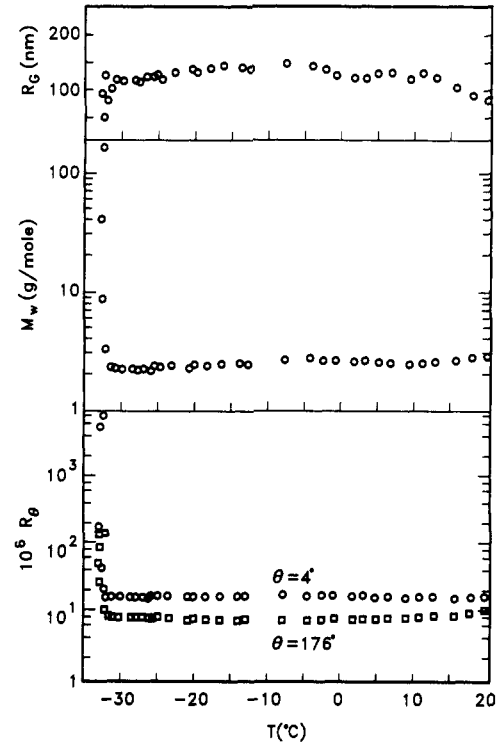

Figure 9. Total scattering (R_θ) at scattering angles 4° and 176°, the calculated M_w, and R_g for C6C6 in hexane at 0.017 mg/mL as a function of temperature.

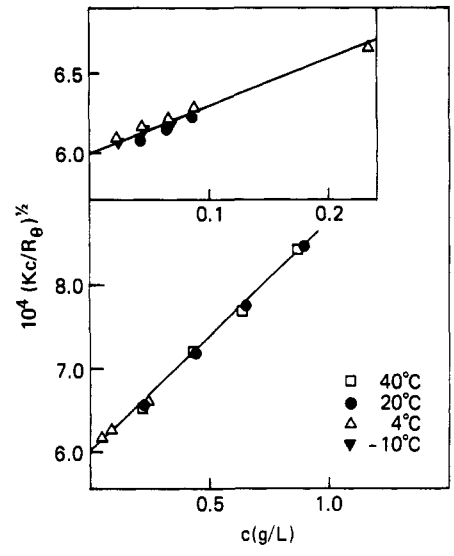

Figure 10. $[Kc/R_\theta]^{1/2}$ versus c for C6C6 in hexane for -10 °C < T < +40 °C.

example in polystyrene solutions in cyclohexane below the Θ-temperature. This may also be observed in the strong dependence of A_2 in this temperature regime. Light scattering measurements of C6C6 in hexane for -7 °C < T < 25 °C (Figure 10) indicate that hexane is a very good solvent for the C6C6 polymer in the thermodynamic sense. A constant value for A_2 was observed, independent of temperature. Hexane may thus be considered nearly an *athermal* solvent, and the phase separation observed at low temperatures is not indicative of an UCST with an amorphous precipitate but is due to an ordering process analogous to crystallization.

Estimation of the d ln $\langle r^2 \rangle$/dT for C6C6 in hexane was accomplished by measurement of R_g for -7 °C < T < 25 °C, as shown in Figure 11, yielding -1.2×10^{-3} K^{-1}. These measurements of R_g were done at several concentrations and extrapolated to infinite dilution to yield the data shown

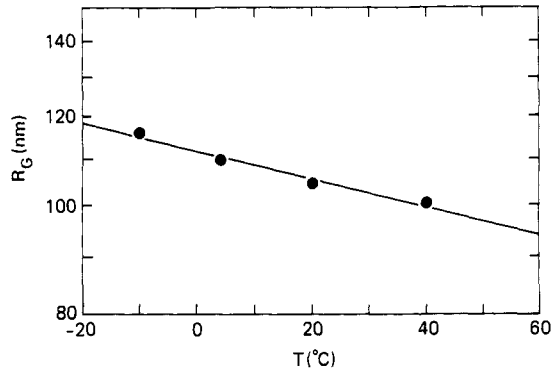

Figure 11. R_g versus T for C6C6 in hexane.

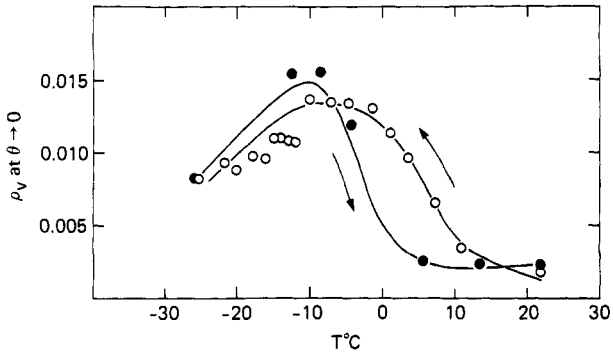

Figure 12. ρ_V as a function of temperature for C6C6 in hexane.

in Figure 11. In this temperature region there is no evidence of any intermolecular or intramolecular association. While determination of d ln $\langle r^2 \rangle / dT$ is more frequently accomplished with stress–temperature coefficients, light scattering may be used in athermal solvents, where excluded-volume interactions are nearly independent of temperature. The increase in this limited temperature range is similar to that observed for other polymers[40] and is not indicative of any unusual conformational transitions. In this temperature range the UV spectra show small red shifts as the temperature is lowered, which also indicate a gradual decrease in the rotational freedom.

Depolarized light scattering measurements were also carried out for C6C6 in hexane as the temperature was lowered through the region where the thermochromic behavior is observed in the electronic absorption spectrum, and the results are shown in Figure 12. The depolarization ratio, ρ_V

$$\rho_V \equiv R_{0,H}/R_{0,V} \tag{25}$$

where the subscripts V and H indicate excess Rayleigh factors measured with vertical and horizontal positions of the analyzer, was measured for C6C6 in hexane at c = 0.174 g/L at a scattering angle of 4°. The values for ρ_V in Figure 12 are quite small and were ignored in the calculation of molecular parameters in Table II. However, the values for ρ_V do increase substantially as the temperature is lowered, reaching a maximum at T = −10 °C when the scattered intensity begins to increase for this concentration. The value of R_g changes very little through this range of temperature. The increase in the depolarized scattering accompanied by little change in R_g can only be consistent with a *local* increase in the *segmental* anisotropy. An increase in the average length of an all-trans segment could result in both a red shift in the electronic absorption maximum and an increase in optical anisotropy.

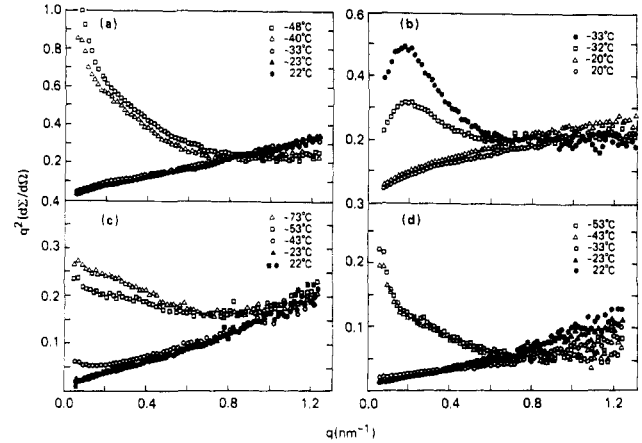

Figure 13. $q^2(d\Sigma/d\Omega)$ versus q (Kratky plots) for the indicated temperatures for C3C6 at 1% (c), C5C6-L at 1% (a), and C5C6-H at 1% (b) and 0.5% (d).

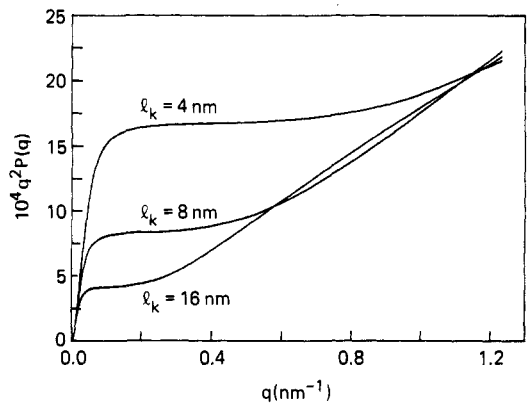

Figure 14. $q^2P(q)$ versus q from the Koyama expressions for the wormlike chain for three values of l_k.

Figure 13 contains the Kratky plots of the neutron scattering for C5C6-L, C5C6-H, and C3C6, at all the temperatures measured, as indicated. In all cases, as the temperature approaches the region where the electronic absorption band narrows, the intensity of the scattering increases dramatically, and the Kratky plot can no longer be interpreted in terms of an average particle scattering function. Although the neutron scattering measurements are carried out at a much higher concentration than the UV spectra, the light scattering measurements at high dilution also showed evidence of aggregate formation.

The functions $P(q)q^2$ vs q (Kratky plots) for different l_k are shown in Figure 14, where $P(q)$ is calculated from the Koyama expression, eq 17. As the temperature is reduced, an uncoiling of a polymer chain to a more extended form is reflected as an increase in the persistence length l_{pers}, or equivalently, the Kuhn length l_k. As may be seen in Figure 14, this results in a decrease in scattering intensity as the transition to the asymptotic rodlike q^{-1} dependence occurs at lower q. The experimental data in Figure 13 for C5C6 do not show this behavior and in fact show an *increase* in intensity at lower q. In Figure 13b, a maximum is observed in the Kratky plot of the scattering from the aggregated solution at low temperatures. This type of scattering behavior is usually observed for more compact particles such as stars, microgel particles, or even ring polymers.[26] In most cases, the maximum occurs at $q^2R_g^2 \approx 2$, so that the data in Figure 13b suggest that the aggregates are quite compact. This is consistent with a "collapsed" aggregate in which intersegmental ordering or crystallization has occurred and with the shrinkage observed in R_g prior to the aggregation for C6C6 shown

in Figure 9. These observations suggest an *intra*molecular association, which may be expected to occur concomitantly with the *inter*molecular association leading to aggregation.

Discussion

Light scattering studies indicate the absence of any dramatic conformational changes, such as a coil-to-rod transition, as the temperature is lowered to the transition point. At very high dilution, a shrinkage of the R_g can be detected near the transition temperature. At higher concentrations aggregation is seen for all three polymers near the transition temperatures. These observations are consistent with the expectation that conformational changes occurring with decreasing temperature for the organosilane polymers are induced by a local ordering occurring through a gradual loss of rotational freedom. Thus the effect is *short-range* rather than *long-range*, and molecular parameters that primarily reflect the most external segments of the polymer segment distribution, such as R_g, are far less sensitive than spectroscopic measurements. The situation is analogous to that observed for biopolymers such as poly(glutamic acid), which may be described globally as a random coil while containing regions of helical segments, which may be detected by circular dichroism.

At temperatures very near to the UV transition, but prior to the onset of aggregation, the R_g of C6C6 in very dilute solutions *decreases*. These observations are consistent with the occurrence of intramolecular associations as well as the intermolecular associations that produce multimolecular aggregates. Recent fluorescence studies at even higher dilutions (10^{-6} M repeat units) indicate that the transition in the electronic absorption spectrum can occur in the absence of intermolecular associations.[41] The *local* polymer segment concentration within a coil remains at around 1 mg/mL even at higher dilution. The polydiacetylenes are a group of polymers that also show thermochromic behavior associated with the formation of intermolecular aggregates. For the polydiacetylenes, spectral transitions may be induced by lowering the thermodynamic quality of the solvent, thermally or by addition of nonsolvent.[10,20,22] The polydiacetylene solutions, which have evidence of aggregation, do not show any concomitant increase in the depolarized scattering.[10] Recent resonance Raman scattering in extremely dilute (10^{-8} M repeat units) solutions of polydiacetylenes demonstrates that the similar transitions observed for these polymers can occur unimolecularly. However, these authors conclude that an *intra*molecular "aggregation" or crystallizationlike process occurs rather than a transition to a fully extended rodlike conformation.[21] This conclusion is also indicated for the polysilanes studied here. No evidence for formation of a rodlike species is found as the temperature is lowered from 20 °C down through the region of the UV transition.

References and Notes

(1) Miller, R. D.; Michl, J. *J. Chem. Rev.* **1989**, *89*, 1359.
(2) Miller, R. D.; Hofer, D.; Rabolt, J. F.; Fickes, G. N. *J. Am. Chem. Soc.* **1985**, *107*, 2172.
(3) Trefonas, P., III; West, R.; Miller, R. D.; Hofer, D. *J. Polym. Sci., Polym. Lett. Ed.* **1983**, *21*, 823.
(4) Pitt, C. G. In *Homoatomic Rings, Chains and Macromolecules of the Main Group Elements*; Rheingold, A. L., Ed.; Elsevier: New York, 1977.
(5) Harrah, L. A.; Ziegler, J. M. *J. Polym. Sci., Polym. Lett. Ed.* **1985**, *23*, 209.
(6) Trefonas, P., III; Damewood, J. R., Jr.; West, R.; Miller, R. D. *Organometallics* **1985**, *4*, 1318.
(7) Hofer, D. C.; Miller, R. D.; Willson, C. G. *Proc. SPIE Adv. Resist Technol.* **1984**, *469*, 108.
(8) Schilling, F. C.; Bovey, F. A.; Lovinger, A. J.; Ziegler, J. M. In *Silicon-Based Polymer Science*; Ziegler, J. M., Fearon, F. W. G., Eds.; American Chemical Society: Washington, DC, 1990; p 341.
(9) Schweizer, K. S. *Chem. Phys. Lett.* **1986**, *125* (2), 118.
(10) Rawiso, M.; Aime, J. P.; Fave, J. L.; Schoot, M.; Müller, M. A.; Schmidt, M.; Baumgartl, H.; Wegner, G. *J. Phys. (Fr.)* **1988**, *49*, 861.
(11) Aime, J. P.; Bargain, F.; Fave, J. L.; Rawiso, M.; Schott, M. *J. Chem. Phys.* **1988**, *89* (10), 6477.
(12) Lim, K. C.; Fincher, C. R., Jr.; Heeger, A. J. *Phys. Rev. Lett.* **1983**, *50* (24), 1934.
(13) Allegra, G.; Brueckner, S.; Schmidt, M.; Wegner, G. *Macromolecules* **1986**, *19*, 399.
(14) Cotts, P. M.; Miller, R. D.; Trefonas, P. T.; West, R.; Fickes, G. N. *Macromolecules* **1987**, *20*, 1046.
(15) Cotts, P. M. *Proceedings of Polymeric Materials, Science and Engineering Division*; American Chemical Society: Washington, DC, 1985; Vol. 53, p 336.
(16) Cotts, P. M.; Maxka, J.; Miller, R. D.; West, R. *Polym. Prepr. (Am. Chem. Soc., Div. Polym. Chem.)* **1987**, *28* (1), 450.
(17) Cotts, P. M.; Dagli, G.; Pearson, D.; Ferline, S., in preparation.
(18) Cotts, P. M.; Miller, R. D.; Sooriyakumaran, R. In *Silicon-Based Polymer Science*; Ziegler, J. M., Fearon, F. W. G., Eds.; American Chemical Society: Washington, DC, 1990; p 397.
(19) Walraff, G. M.; Baier, M.; Miller, R. D.; Rabolt, J. F.; Hallmark, V.; Cotts, P.; Shukla, P. *Polym. Prepr. (Am. Chem. Soc., Div. Polym. Chem.)* **1989**, *30* (2), 245.
(20) Müller, M. A.; Schmidt, M.; Wegner, G. *Makromol. Chem., Rapid Commun.* **1984**, *5*, 85.
(21) Taylor, M. A.; Odell, J. A.; Batchelder, D. N.; Campbell, A. J. *Polymer* **1990**, *31*, 1116.
(22) Wenz, G.; Müller, M. A.; Schmidt, M.; Wegner, G. *Macromolecules* **1984**, *17*, 837.
(23) Kim, S.; Cotts, P. M. *J. Appl. Polym. Sci.* **1991**, *42*, 217.
(24) Flory, P. J. *Principles of Polymer Chemistry*; Cornell University Press: Ithaca, NY, 1959; p XX.
(25) Yamakawa, H. *Modern Theory of Polymer Solutions*; Harper and Row: New York, 1971; p 359f.
(26) Burchard, W. In *Advances in Polymer Science*; Springer-Verlag: Berlin, Heidelberg, 1983; p 67f.
(27) Koppel, D. E. *J. Chem. Phys.* **1972**, *57*, 4814.
(28) Reference 25, p 218f.
(29) Rochefort, W. E.; Heffner, G. W.; Pearson, D. S.; Miller, R. D., Cotts, P. M. *Macromolecules*, in press.
(30) Schmidt, M.; Nerger, D.; Burchard, W. *Polymer* **1979**, *20*, 582.
(31) Kajiwara, K.; Burchard, W. *Macromolecules* **1984**, *17*, 2674.
(32) Kajiwara, K.; Burchard, W. *Macromolecules* **1984**, *17*, 2669.
(33) Kratky, O.; Porod, G. *Recl. Trav. Chim. Pays-Bas* **1949**, *68*, 1106.
(34) Sharp, P.; Bloomfield, V. *Biopolymers* **1968**, *6*, 1201.
(35) Koyama, R. *J. Phys. Soc. Jpn.* **1973**, *34* (4), 1029.
(36) Yoshizaki, T.; Yamakawa, H. *Macromolecules* **1980**, *13*, 1518.
(37) Holtzer, A. *J. Polym. Sci.* **1955**, *17*, 432.
(38) Schmidt, M.; Paradossi, G.; Burchard, W. *Makromol. Chem., Rapid Commun.* **1985**, *6*, 767.
(39) Kuzmany, H.; Rabolt, J. F.; Farmer, B. L.; Miller, R. D. *J. Chem. Phys.* **1986**, *85*, 7413.
(40) Flory, P. J. *Statistical Mechanics of Polymer Chains*; Interscience: New York, 1969; p 44f.
(41) Sun, Y.-P.; Miller, R. D.; Sooriyakumaran, R.; Michl, J. *J. Inorg. Organomet. Chem.* **1991**, *1*, 3.

Registry No. C_3C_6, 125121-31-5; C_5C_6, 120517-00-2; C_6C_6, 94904-85-5; THF, 109-99-9; hexane, 110-54-3; neutron, 12586-31-1.